

BINDURA UNIVERSITY OF SCIENCE EDUCATION

**FACULTY OF SCIENCE AND ENGINEERING
DEPARTMENT OF CHEMISTRY**



**FRUIT JUICE CARBON DOTS, ZINC OXIDE COMPOSITE FOR
PHOTOCATALYTIC DEGRATION OF ORGANIC POLLUTANTS**

LOVENESS CHITARE

REG: B190598B

SUPERVISOR: Dr W MUNZEIWA

**A RESEARCH PROJECT SUBMITTED IN PARTIAL FULFILMENT OF
THE REQUIREMENTS OF BACHELOR OF SCIENCE HONOURS
DEGREE IN CHEMICAL TECHNOLOGY(HBScCHT)**

30 May 2023

APPROVAL FORM


The signatures below certify that they have supervised, read and recommend to the Bindura University of Science Education for acceptance as a research project entitled:

FRUIT JUICE CARBON DOTS, ZINC OXIDE COMPOSITE FOR PHOTOCATALYTIC DEGRATION OF ORGANIC POLLUTANTS

Submitted By: LOVENESS CHITARE

Reg No: B 190598 B

In partial fulfilment of the requirements for the BACHELOR OF SCIENCE HONORS DEGREE
IN CHEMICAL TECHNOLOGY

 /30/05/2023

(Signature of Student) (Date)

 / 03 / 10 / 2023

(Signature of Supervisor) (Date)

 04 /10 / 2023 / / /

(Signature of chairperson) (Date)

DECLARATION FORM

I, CHITARE LOVENESS, declare to Bindura University of Science Education that this dissertation is my original work, and that all materials and academic sources of information have been properly acknowledged. This work has not been submitted to any other academic institution for academic consideration.

Signed  ...Date ...30/05/2023....

DEDICATION

This academic work is dedicated to Esther Chitare, Angeline Chitare, and Emmanuel Chitare.

ACKNOWLEDGEMENTS

Greater thanks to Dr Munzeiwa for his supervision, invaluable knowledge, support, contribution, patience and academic information which all facilitated to the success of this project. I also acknowledge the BUSE laboratory staff for their expertise, kindness, help and advice. My profound gratitude goes to my parents who gave me financial and motivational support towards my education. All their efforts were not in vain.

LIST OF ABBREVIATIONS

CQDs	Carbon Quantum Dots
PL	Photoluminescence
FTIR	Fourier Transform Infrared
UV	Ultra Violet
ZnO/CQDs	Zinc oxide/ Carbon Quantum Dots
MB	Methylene Blue
BOD	Biological Oxygen Demand
COD	Chemical Oxygen Demand
IR	Infrared Red

LIST OF FIGURES

Figure 2.1 illustration of photocatalytic degradation mechanism of organic contaminants (dyes)	8
Figure 2.2 preparation of CQDs from lemon juice by hydrothermal treatment (He et al., 2018)	13
Figure 2.3 Types of adsorption isotherms (Chahal 2016)	15
Figure 4.1 showing result of CQDs when observed in (a) daylight (b)UV radiation (c)Fluorescence radiation	25
Figure 4.2 showing the FTIR spectra of the three synthesized CQDs	27
Figure 4.3 showing the % degradation of methyl blue with different catalysts	28
Figure 4.4 effect of temperature on the photodegradation of methyl blue	29
Figure 4.5 effect of pH on the photodegradation of methyl blue	30
Figure 4.6 effects of time on the photodegradation of methyl blue.....	31
Figure 4.7 effects of catalyst dosage on the photodegradation of methyl blue	32
Figure 4.8 data analysis for[a] Langmuir and [b] Freundlich isotherms	33
Figure 4.9 data on Reactin kinetic	34
Figure 4.10 data showing thermodynamic parameters	36

LIST OF TABLES

Table 2.1 sources of CQDs	10
Table 4.1 physical characteristics of the photocatalyst	26
Table 4.2 adsorption isotherm parameters and reaction kinetics parameters	35
Table 4.3 thermodynamic parameters	36
Table 4.4 the photocatalytic activity of ZnO/CQDs comparison with other different photocatalysts for methy blue degradation in recent years	37

Contents

APROVAL FORM	i
DECLARATION FORM	ii
DEDICATION	iii
ACKNOWLEDGEMENTS	iv
LIST OF ABBREVIATIONS	v
LIST OF FIGURES	vi
LIST OF TABLES	vii
CHAPTER 1	1
1.1 ABSTRACT	1
1.2 BACKGROUND	1
1.3 Problem Statement	3
1.4 Aims	3
1.5 Specific Objectives	3
1.6 Problem Justification	4
1.7 Project scope	4
1.8 Significance of research	4
Chapter 2	5
2.0 Literature Review	5
2.1 Definition of key words	5
2.2 Zinc oxide and its composite to CQDs	5
2.3 Photocatalytic technology	6
2.3.1 Photocatalytic degradation mechanism using ZnO/CQDs	7
2.3.2 Factors affecting degradation performance of the organic contaminants	8
2.4 Carbon Quantum Dots sources	10
2.4.1 Lemons	11
2.5 Synthesis of CQDs	12
2.5.1 Top-down methods	12
2.5.2 Bottom-up methods	12
2.6 Characteristics of CQDs	13
2.6.1 Photoluminescence	13

2.6.2 Photostability.....	14
2.7 Characterization methods	14
2.7.1 Transmission electron microscope	14
2.7.2 X-Ray diffraction spectroscopy	14
2.7.3 UV/Vis spectroscopy	14
2.7.4 FT-IR spectroscopy.....	15
2.8 Adsorption Isotherms.....	15
2.8.1 Langmuir isotherm	16
2.8.2 Freundlich Adsorption Isotherm.....	17
2.9 Kinetic Studies	18
2.9.1 Pseudo First Order Model	18
2.9.2 Pseudo Second Order Model	18
2.10 Organic pollutant literature.....	19
Chapter 3.....	20
3.0 Materials and Methodology	20
3.1 Reagents and Apparatus	20
3.2 Synthesis of Carbon Quantum dots	20
3.3 Synthesis of Zinc oxide	20
3.4 Synthesis of CQDs/ Zinc Oxide Composite	21
3.5Preparation of water polluted with organic pollutants	21
3.6 Characterization Methods	21
3.6.1 UV/ Vis spectrophotometer Analysis	21
3.6.2 FT-IR Spectrophotometer Analysis	21
3.6.3 Transmission Electron Microscope.....	22
3.9 Photocatalytic Degradation Of methylene blue	22
3.10 Data treatment methods.....	23
3.10 Removal capacity and adsorption capacity	23
3.11 Model fitting analysis	23
3.11.1 Adsorption Isotherms	23
3.11.2 Kinetic Studies.....	24
3.11.3 Thermodynamics studies.....	24
Chapter 4.....	25
4.0 Results and discussion	25

4.1 Physicochemical analysis	25
4.1.1 Synthesis	25
4.1.2 pH_{zpc} analysis.....	26
4.3 photocatalytic degradation of methyl blue	27
4.4 Optimization parameters	28
4.4.1 effect of temperature	28
4.4.2 Effect of pH	29
4.4.3 Effect of adsorption time	30
4.4.4 Effect of photocatalyst dosage	31
4.5 Model fitting analysis	32
4.5.1 Adsorption isotherms	32
4.5.2 Reaction kinetics (pseudo).....	34
4.5.3 Thermodynamic study.....	35
4.6 Comparative study.....	36
4.7 Photodegradation mechanism and reaction scheme.....	37
Chapter 5.....	39
5.1 Conclusion	39
5.2 Recommendations.....	39
References.....	40
Appendix.....	44

CHAPTER 1

1.1 ABSTRACT

To create a composite photocatalyst (ZnO/CQDs) for the breakdown of methyl blue, the CQDs from citrus juice (lemon) by hydrothermal synthesis were combined with ZnO produced via the precipitation method using the incubation technique. The main goal of the composite photocatalyst were to lessen the drawbacks of conventional quantum semiconductors employed in the photocatalytic decay of organic contaminants. The ZnO /CQDs composite photocatalysts formed were characterized by adsorption- desorption isotherms, FTIR and UV/Vis spectrophotometer calibration curve of MB (methyl blue) was plotted before catalysis process. Optimization parametric variables for example pH, temperature, contact time and catalyst dosage were conducted to ensure high efficiency in the photo-oxidation procedure. The degradation processes for the organic contaminant were conducted in a laboratory scale in a small reactor cell surrounded by UV lights. Composite ZnO/CQDs₆ was used in the catalysis process which had the highest rate of degradation of 95.04%. This study uses that Langmuir adsorption isotherm and follows the pseudo-first order. The reaction process was spontaneous and endothermic as evidenced by thermodynamic results.

1.2 BACKGROUND

In 2004, Xu et al. developed a unique class of nanoscale carbon-based materials known as carbon dots (CD), with a spatial dimension smaller than 20 nm. (Xu et al., 2004). In the year 2006, Sun et al. created the luminous carbon nanoparticles and named them "carbon quantum dots (CQDs)" from being carbon dots, using the laser ablation technique from graphite powder. The CQDs were formulated by combining different carbon precursors, namely glucose (Hallaj, Amjadi, Manzoori, et al., 2015), citric acid (Dong, Shao, Chen, et al., 2012), and vitamin C (Wang et al., 2012). Citrus fruits such as Citrus limon have proven to be much effective sources in which CQDs can be formulated from, which have a wide range of useful uses industrially (Chatzimitakos et al., 2017).

Zinc oxide is an excellent catalyst I the field of photocatalysis of organic pollutants. However, ZnO have larger band gap of 3.37 eV, and is considerably higher and limits its light absorption ability in the ultra violet region only and decreases the activity efficiency of the photocatalyst (Meshram et al., 2017). Despite this drawback, ZnO band gap may be changed at the nanoscale to enhance the reflective characteristics of zinc oxide (Yibeltal et al., 2020). To counter this

drawback CQDs, because they have very good optical and electrical characteristics, and to add to that these nanostructured carbon-based materials have good biocompatibility, low toxicity, and high-water solubility have been used significantly for this use (Ding et al., 2016, Shen et al., 2012). Numerous related basic and applied research projects have been carried out globally on CQDs (Ramanan et al., 2016). These outstanding qualities make them the best possible candidates for use in the photocatalysis industries, biological industries and, optoelectronic industries (Bozetine et al., 2020).

In this current work, lemon juice in the major carbon source, and CQDs were produced using hydrothermal processing. The CQDs prepared by hydrothermal processing of lemon juice were employed to create a nanocomposite with ZnO. In fact, the promotion of photogenerated electrons from the valence band to the conduction band occur to a greater extent when ZnO was impregnated with CQDs. These CQDs were prepared varying the reaction time for the carbonization of common organic compounds such as vitamin C and citric acid found in lemon juice and used to formulate three different ZnO/CQDs nanocomposites namely ZnO/CQDs₂, ZnO/CQDs₄, and ZnO/CQDs₆, which were used for the degradation of methylene blue dye found in industrial waste water or other aqueous environment.

According to Chu et al. (2019), the CQDs/photocatalysts composite was produced either by one-pot or multi-step synthesis technique. The multi-step procedure involves either adding to the photocatalyst, a solution of pre-made carbon dots, or incubating carbon dots and zinc oxide nanoparticles. In one-pot synthesis all of the initial components for CQDs, photocatalysts, and composites are combined in a single pot for subsequent processing (Chu et al., 2019).

The transmission electron microscope (JEM 2100, Japan) running at 300 KV is used to examine the morphology and microcrystalline structures of carbon quantum dots made from the citrus lemon juice (He et al., 2018). A UV-Vis spectrophotometer (Specord200) was used to measure the UV-Vis absorption spectra. Shimadzu FT-IR 8400S, a Japanese FTIR, and Perkin Elmer Instruments version 3.02.01 software were used to analyze the spectrum composition of the primary functional groups present on the nanostructured ZnO/CQDs composite materials .

The photocatalytic properties of the synthesized nanocomposites photocatalysts gave different results with ZnO/CQDs₆ having higher performance in comparison with ZnO/CQDs₄ and

ZnO/CQDs². Thus the excellent performance was due to the different abilities of the nanostructured composite in reducing the reflective characteristics of ZnO nanoparticles which resulted in different abilities of the n ZnO/CQDs nanocomposites light absorption in the visible range of the spectrum.

1.3 Problem Statement

The use of traditional fluorescent semiconductor quantum dots such as CdS, TiO₂, WO₃, NiO, and ZnO, during the photocatalytic conversion of organic compounds to carbon dioxide and water have numerous drawbacks which include, cytotoxicity caused by using heavy metals, environmental hazard, potential health and high cost. However, each photocatalyst tend to have its own band gap energy and different photooxidation capability (Augugliaro et al., 2012). For photocatalyst with high energy gap such as that of zinc oxide, the photon absorption efficiency is low owing to reduced catalytic activity. Hence the need for doping of the photocatalyst with carbon quantum dots nanoparticles to counter the limitations and improve capability of photooxidation of the organic contaminants produced by various industries

1.4 Aims

- synthesis of zinc oxide/carbon quantum dots nanoparticle composites used for photodegradation of organic pollutants

1.5 Specific Objectives

- to synthesize carbon quantum dots from lemon juice and form composite catalyst with ZnO
- To characterize the synthesized composite zinc oxide/carbon quantum dots using transmission electron microscope, UV/ Vis spectrophotometer, and FTIR
- To apply CQDs/photocatalyst composite in photocatalytic degradation of organics
- To evaluate the efficiency of the photocatalytic degradation of the organic pollutants with different photocatalyst.
- To study the adsorption isotherms, kinetic data and thermodynamics of the reaction.

1.6 Problem Justification

Carbon dots are being looked at as prospective replacements for conventional fluorescent semiconductor quantum dots, which have a number of drawbacks, including heavy metal toxicity, a risk to human health and the environment, and uneconomic (Kuan-wu., 2019). Moreover, their hybridization with TiO₂, Ag₃PO₄, ZnO, SiO₂, Cu₂O and Fe₂O₃, is described as the innovative discovery to boost charge separation and reduce charge recombination, while increasing the rate of photocatalytic oxidation efficiency as a result (Muthulingam et al., 2015; Lu et al. 2012).

1.7 Project scope

- The scope of all materials, equipment and analytical references to the experimental work and analysis to be carried out depends on the available resources.

1.8 Significance of research

- Preservation of flora and fauna.
- To safeguard the human health factor.
- Adherence to Environmental management agency's regulatory standards, thereby sidestepping payment of fines.

Chapter 2

2.0 Literature Review

2.1 Definition of key words

Carbon quantum dots

Bright photoluminescent quasi-spherical carbon nanomaterials, which are mostly composed of graphitic sp² and sp³ carbon hybridization with sizes less than 10 nm, and are a novel type of carbon nanomaterials (Zheng et al., 2015).

Photocatalyst

A photocatalyst is a design of matter that has a consistent chemical composition and characteristic properties made up of photons that can excite a reaction without being consumed. It is most commonly used as a power-harvesting master (Fox., 2010)

2.2 Zinc oxide and its composite to CQDs

Zinc oxide is a white solid with the molecular mass of 81.38 g/mol. ZnO exist in two main structures which are hexagonal and cubic structures but the hexagonal structure is most common and stable. Zinc oxide have a variety of application both in medical and industrial field and one of its applications being that it can be used as a catalyst. Zinc oxide has excellent photocatalytic oxidation capacity in photodegradation of organic pollutants producing carbon dioxide and water as the main end products.

Due to its outstanding performance in environmental applications like the purification of effluents or contaminated air, zinc oxide (ZnO) gained some interests and one of them is use as a photocatalyst (Djurisi et al., 2012). Additionally, its great photosensitivity is closely related to other crucial characteristics including its non-toxicity and inexpensive price (Djurisi et al., 2012),. However, obstacles to its broad use include its high bandgap of 3.37 eV, substantial charge carrier recombination, and photoinduced corrosion-dissolution severe pH environments, resulting to inert Zn(OH)₂ (Kuma et al., 2015).

To enhance the photocatalytic efficiency of zinc oxide additional CQDs are added forming composite photocatalyst which reduced most of the adverse effects of using the semiconductor catalyst alone. Due to their large specific surface area, carbon quantum dots facilitate the adsorption of contaminants on to photocatalyst surface and promotes the separation and transport of photogenerated electron-hole pairs (Lin et al., 2020; Zou et al., 2021). The CQDs also enhance the cycle stability of the degradation process and lowers the likelihood of photogenerated holeelectron pair recombination.

When CQDs and ZnO are combine they interact by forming electrical interactions, as a result the composite photocatalyst formed have greater ability for charge separation and reduce charge recombination. Accordingly, proof has been provided that the inherent characteristics of ZnO/CQDs and the photocatalytic activity are correlated (Toma et al., 2022). The advantages of CQDs in the composite photocatalyst are as follows:

- High water dissolution
 - Low cytotoxicity
 - Good biocompatibility
 - Highly stable
 - outstanding water dispersibility and photostability
- (Rani et al., 2020)

2.3 Photocatalytic technology

Photocatalytic technology is a process of converting photonic energy (from solar irradiation) to chemical energy by using photocatalyst. The malignant organic contaminants in water or air are converted to water, carbon dioxide and detritus. The technology is a green chemistry approach which deals with pollution control and removal of organic pollutants such as antibiotics, organic dyes and agrochemicals thereby reducing their effects on both humans and terrestrial environment at large. The main aim of this approach is to find different ways which enhance photocatalytic efficiency and stability of different photocatalyst (Tan et al., 2022, Abderrahim et al., 2022). Recently photocatalytic technology has invoked carbon quantum dots in photocatalysis of organic compounds as a way to reduce the adverse effects of the traditional semiconductor's quantum dots. These CQDs dots can be used alone in photocatalysis or they can be combined with the

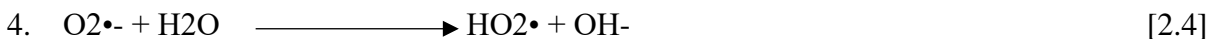
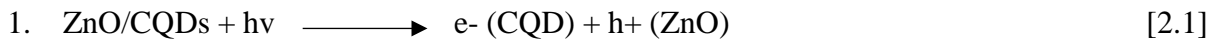
convectional semiconductor quantum dots forming composite photocatalyst which are more efficient and pollutant free to the environment.

Henceforth Carbon quantum dots (CQDs) a novel group of carbon nanostructures can be used to improve the photocatalyst ZnO efficiency in photocatalytic degradation of organic pollutants. These nanoparticles have elements such as carbon, nitrogen, hydrogen, and oxygen, and these elements are structured into different functional groups, which makes them capable of dissolving in water (Sharma, 2017). Due to their good photoluminescence properties CQDs obtained from lemon juice have a lot of application in the biological and chemical field one of which is the photocatalytic degradation of organic pollutants

2.3.1 Photocatalytic degradation mechanism using ZnO/CQDs

Zou and colleagues recently presented a mechanism for photo-degradation of organic dyes utilizing UV light and it matches with this study findings (li, et al 2013). The UV-light focused to the ZnO/CQDs in waste water at energies greater or equivalent to ZnO bandgap energy, electrons will be excited and move from the valence band (VB) to the conduction band (CB). Through a photo-induced charge transfer mechanism, these electrons travel from the CB to the surface layer of the CQDs whereas the positive holes (h⁺) depart from the valence band of ZnO (equation 2.1)

The positive holes (h⁺) move to the surface-layer of the photocatalyst where it reacts with H₂O or OH⁻ producing OH• radicals (equation 2.3). The electrons photonically generated further reacts with oxygen on CQDs surface forming O₂•⁻ radicals (equation 2.2) and then the O₂•⁻ is further protonated releasing hydroperoxyl HO₂• radicals (equation 2.4), generating OH• and hydrogen peroxide (equation 2.5). Hydrogen peroxide is another precursor to OH• radical production (equation 2.6). All the species produced have strong oxidizing power to degrade MB degrade them to CO₂ and H₂O (equation 2.7).



7. $\text{OH}\cdot + \text{dye}$

$\text{CO}_2 + \text{H}_2\text{O}$

[2.7]

(Toma et al., 2022)

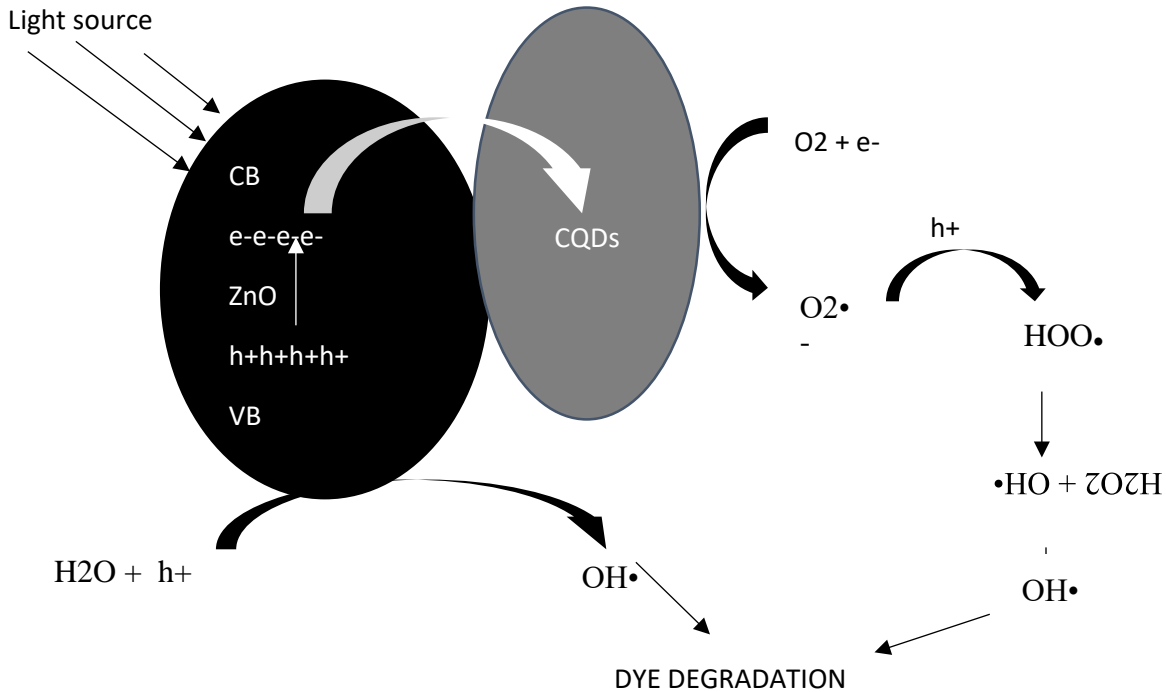


Figure 2.1 illustration of photocatalytic degradation mechanism of organic contaminants (dyes) (Toma et al., 2022)

2.3.2 Factors affecting degradation performance of the organic contaminants

2.3.2.1 The solution pH.

It's quite difficult to extrapolate how pH affects the effectiveness of the photo-oxidation process of organic contaminants. This is because there are three distinct reaction pathways that contribute to photo-oxidation of the dye. These pathways include, the hydroxyl radical attack, direct reduction by the electrons in conducting band and the direct oxidation by the positive holes (Tang et al., 1997). Each one's contribution is affected or induced by pH in a different manner. The pH of the solution alters the electrical double layer of the solid electrolyte interface, which has an impact on the adsorption-desorption processes and affects separation of the photogenerated electron-hole pairs on surface of the photocatalyst (Reza et al., 2015). The solution pH has direct impact on charge of the photocatalyst surface particles, the position of the conduction band and the valence band, and size of aggregates.

2.3.2.2 Size and morphology of the photocatalyst

Considering that the relationship between the surface coverage on the photocatalyst and the size of the organic molecules, surface anatomy, which includes particle size and granule shape, are an essential element to take into account for effective photocatalytic degradation process (Guillard et al., 2003). The photocatalyst's shape and size provide information on total amount of contaminants which will be adsorbed to its surface per unity time. The rate of organic pollutant oxidation increases with increase in surface area.

2.3.2.3 Reaction temperature

Temperature influence on the rate of a photo-degradation activity has been accounted for if the reaction is either endothermic or exothermic. For an endothermic reaction, as temperature increases the rate of the degradation process rises. This can be accounted by, that increase in temperature increase the average kinetic energy and particle collision thereby increasing the rate of reaction. However, higher reaction temperatures can reduce the rate of photocatalytic activity by encouraging recombination of charge carriers and disfavoring adsorption of organic pollutants to the surface of the photocatalyst. Therefore, an optimum temperature for a reaction has to be used for maximum efficiency. For a reaction that is exothermic and spontaneous a decrease in temperature promotes adsorption of the organic pollutants (Khan et al., 2015).

2.3.2.4 Catalyst loading and concentration of the organic pollutants

For a photocatalytic activity reaction, the amount of composite photocatalyst is directly promotional to the degradation rate up until it reaches maximum and then starts to fall with increasing the photocatalyst dose. This is due to the fact that when photocatalyst dose increases, it results in sufficient number of active sites for adsorption of the organic pollutants. However, a photocatalyst dose above saturation level, results in reduced light absorption capacity which is mainly caused by the light screening effect of the excess photocatalyst and results in the reduction in surface area of the catalyst exposed to UV. Excess amount of the photocatalyst have a negative impact on the rate of the degradation process.

2.3.2.5 Light intensity and wavelength of light

The band gap of a photocatalyst affect the region to which it can absorb a photon of light. The rate of degradation process follows a direct proportionality relationship with increasing light intensity, (first order reaction), at low light intensities, the efficiency of the process will rely on the square root of the light intensity (half order reaction) for intermediate levels of light, and when light levels are high, the rate is independent of the level light. More photons per unit time and space improve the likelihood that photons will activate on catalyst surfaces, resulting in increased photocatalytic power. The number of activation sites does not change with increasing light intensity, therefore even when the light intensity rises, the response rate only reaches a specific point (Ollis et al., 1992).

2.4 Carbon Quantum Dots sources

In addition to bulk materials based on carbon such as graphite, carbon quantum dots have been produced from both macromolecules either natural or manufactured and small molecule precursor (Chu et al., 2019). CQDs due to their beneficial effects when formed into composite catalysts with traditional semiconductor quantum dots there is need to look into their sources. The three main groups to which CQDs can be categorized is shown in *table 2.1* shown below. *Table 2.1 sources of CQDs*

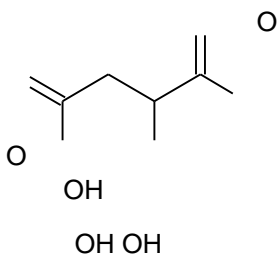
Group	Examples
Natural polymers and biomas	cow milk, egg white, lemons, lignin, peach gum, cashew gum, peanut shell, sweet potato and grass.
Small precursors	citric acid, citrate salts, and acrylic acid, p-phenylenediamine
Synthetic polymers	branched polyethyleneimine, polyacrylamide, polyvinyl alcohol, polyacrylic acid + EDA, polyamidoamine dendrimer

2.4.1 Lemons

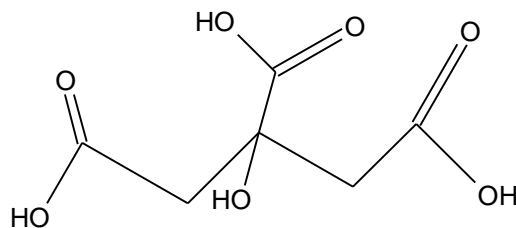
Lemons are yellow oval shaped fruit that belong in the citrus family. The lemon juice contains the following compounds approximately 5% to 6% citric acid, minute amounts of Vitamin B, (niacin, riboflavin, and thiamine), fibers (pectin), minerals and essential oil. Also, lemon juice contains other acids but in small amounts and these include malic acid and vitamin C (ascorbic acid). The pH of a standard lemon juice ranges from 2 to 3.5, this results in the sour taste of lemon juice. In addition, lemon juice contains water (88–89%) in higher amounts and carbohydrates. The carbohydrates are mainly composed of monosaccharides (fructose, glucose) and the disaccharide sucrose. The carbonization of the organic compounds (precursors) found in lemon juice results in synthesis of CQDs via hydrothermal synthesis

Structures of main compound found in lemon juice

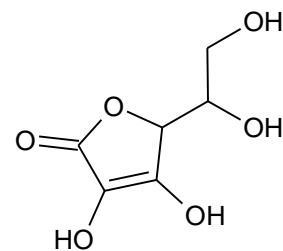
Malic acid



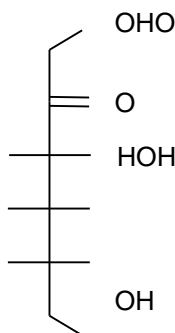
Citric acid



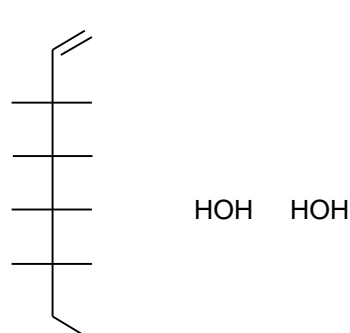
Ascorbic acid (vitamin c)



fructose



Glucose



2.5 Synthesis of CQDs

Top-down methods and the bottom-up approaches were the main groups under which carbon quantum dots can be synthesized utilizing different precursors.

2.5.1 Top-down methods

This technique synthesizes the carbon quantum dots by the carbonization of larger carbon precursors like graphene, graphite and fullerene. The widely used top-down techniques that have the currently used include laser ablation (Sun et al., 2016, Reyes et al., 2016), ultrasonic method (Zhou et al., 2012) and electrochemical oxidation (Yang et al., 2015, Lui et al., 2016). The characteristics which include size and crystalline structure of CQDs are controlled by a one-step route in the synthesis process. Top-down approaches, however, frequently require pricey and complex machines, difficult processing steps, or harsh reaction conditions, and the resultant CQDs' quantum yield (QY) and biocompatibility are not satisfactory. Hence, chemical treatment is frequently used to passivate or alter CQD surfaces after these methods.

2.5.2 Bottom-up methods

In contrast, the bottom-up strategy produces carbon-based nanoparticles by decomposing, fusing, or carbonizing tiny or big precursors. Most widely used bottom-up methods for generating CQDs include the pyrolysis (Ma et al., 2017), ultrasonic treatment (Park et al., 2015), thermal decomposition (Wang et al., 2015), microwave approach (So et al., 2017, Xu et al., 2014), and hydrothermal treatment (Tao et al., 2017, Lu et al., 2012), within others. The precursor materials used in this approach might be tiny or big, and they can be made of polymers that are both natural and artificial. In comparison to top-down techniques, bottom-up methods are simple, economical, and ecologically benign (i.e., the reaction conditions and reagents are favorable), and have broad range of readily accessible precursor units. By altering reaction conditions, optical characteristics of CQDs may be easily modified.

2.5.2.1 Hydrothermal Synthesis Approach

A process called hydrothermal synthesis utilize high pressures and temperature to transforms organic molecules in water into structured carbon quantum dots (Kuan et al. 2019). The hydrothermal approach, has been utilized and favored by many researchers as a mature way of CQD production, has the benefits of being environmentally friendly, non-toxic, inexpensive, and simple to use (Shekarbeygi et al., 2020; Jiang et al., 2020). The solution with the major source of

CQDs is typically cooked for hours at temperatures between 100°C and 220°C after being enclosed within a Teflon-lined autoclave. Then, to get carbon dots that are nanometer-sized, large particles are eliminated. In reality, the hydrothermal method has been the method of choice for creating CQDs from a variety of natural polymers and manmade macromolecules. The illustration of a simple hydrothermal approach is shown in fig 2.2 for the synthesis of CDQS.

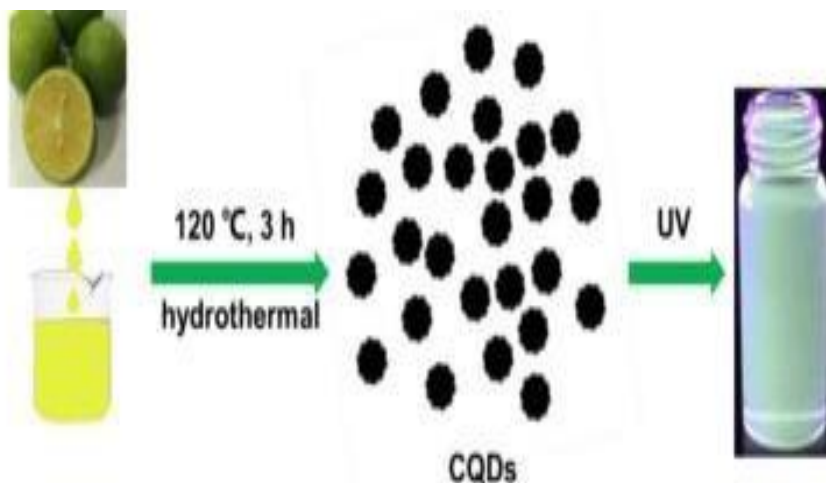


Figure 2.2 preparation of CQDs from lemon juice by hydrothermal treatment (He et al., 2018)

2.6 Characteristics of CQDs

2.6.1 Photoluminescence

Photoluminescence (PL) is the term for the emission of light from any material in response to the absorption of a photon of light (Yadav et al., 2023). This is the most enticing feature of carbon quantum dots. The two types of photoluminescence are phosphorescence and fluorescence. Emission of light from lowest singlet excited state (S1) to singlet ground state (S0), is called fluorescence and in the fluorescence process transition between the electronic states have the same spin multiplicity hence it is an allowed transition. Contrarily, in phosphorescence, a prohibited transition takes place in accordance with the spin selection rule, because the transition is from the lowest triplet excited state (T1) to the singlet ground state (S0) (Yadav et al., 2023). Carbon quantum dots have a broad spectrum of PL emission spectra that can span from ultraviolet to near infrared

2.6.2 Photostability

The primary trait of CQDs (photostability) is influenced by the environment to which it is exposed to. CQDs are highly stable and they should be stored under cool conditions (temperature below 25 °C and no exposure to sunlight). However, exposure under harsh environmental conditions causes aggregation and lattice degradation that is related to a disruption of the fluorescence characteristics (Sidhu et al., 2017). It is consistent with earlier stability analyses (Wang et al., 2017; Dager et al., 2019) that light causes a very slight drop in fluorescence intensity. Fluorescence emission drops and the stability of CQD decreases as temperature rises. Contrary to amorphous CQDs, crystalline CQDs may have exceptional photostability (Liu et al., 2017; Nie et al., 2020).

2.7 Characterization methods

2.7.1 Transmission electron microscope

Transmission electron microscope (TEM) is a microscopic method which provides high-resolving power when analyzing carbon nanostructures. The TEM machine consist of an electron source found on top of the machine and is capable of emitting electrons which moves through a vacuum in the column of the machine. They are also electromagnetic lenses which concentrates electrons through a small beam and these electrons are focused onto the sample. A signal will be produced by the detector after the electrons were focused on to the sample.

2.7.2 X-Ray diffraction spectroscopy

The most well-known and widely utilized approach for determining the atomic and molecular structures of materials is x-ray diffraction. The crystalline atoms cause the x-beam bar to diffract in specific directions. As a result, the diffraction spots and intensities may be measured and recorded, resulting in a 3-D representation illustrating how thick the electrons inside the crystal are. The XRD- approach has the following advantages: it requires a small amount of sample, it is non-destructive, and it is simple to interpret (Donia, et al., 2015).

2.7.3 UV/Vis spectroscopy

UV-vis spectroscopy is a method widely applied to survey the photosensitive characteristics of many-sized particles. When light is focused through the specimen the quantity of light absorbed is measured and recorded. UV/Vis spectroscopy also measures the amount of the adsorbed light in a wide range of wavelength. The concentration of a solution can be determined using beer-lambert's

law using the absorbance in the spectra (Ribeiro and Nunes, 2011). Also, the spectroscope can be used to plot calibration curves of different standard solutions.

2.7.4 FT-IR spectroscope

Fourier Transform Infrared Spectroscopy (FTIR) is an analytical technique used to analyze common functional groups that make up carbon-based compounds or in other instances inorganic complexes. The absorption bands in the infrared spectrum of the spectra indicate molecular structures (Griffiths, 2006). The absorbed infrared (IR) radiation in general stimulates molecules to higher vibrational states when a substance is bombarded with the IR. Energy difference between the stimulated vibrational states and the at rest state alludes the wavelength of absorbed light by a specific fragment of molecule (Griffiths, 2006). The molecular structure of the sample is indicated by the wavelengths a sample absorbs.

2.8 Adsorption Isotherms

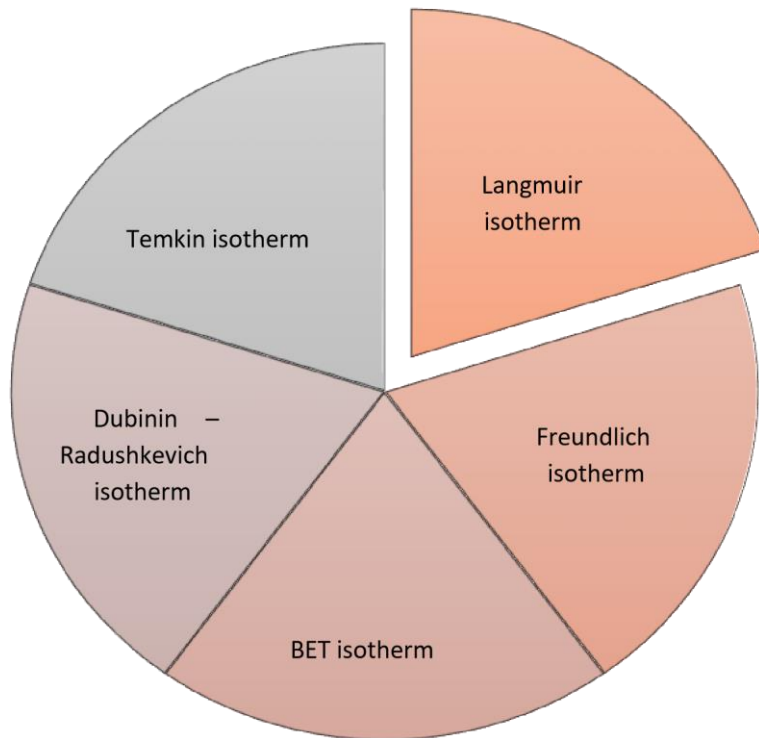


Figure 2.3 Types of adsorption isotherms (Chahal, 2016)

Adsorption isotherms gives literature on relationship on the equilibrium concentration of the pollutants on the adsorbent, and quantity of adsorbate adsorbed on surface at constant temperature. The different types of adsorption isotherms are shown in Fig 2.2.

2.8.1 Langmuir isotherm

The Langmuir isotherm operates basing on the three assumptions below:

- Catalyst surface with adsorbing sites is a perfectly uniform and the adsorption sites are the same.
- The adsorption of a substrate to catalyst surface does not affect the adsorption of other molecules
- Adsorption cannot go beyond the mono-layer coverage (Atkins et al., 2010)

The free substrate and adsorbed substrate exist in dynamic equilibrium. Attachment of substrate to the adsorbent surface can either be chemisorption or physisorption. When the attachment is via covalent bond it is known as chemisorption and when interaction is via Van Der Waals it is known as physisorption. (Ramachandran et al., 2011). The enthalpy change of chemisorption is higher while the process is irreversible and the enthalpy change of formation for physisorption is lower and the process is reversible (Atkins et al., 2010).

Langmuir isotherm linear form is denoted by equation (2.8) below:

$$\frac{C_e}{Q_e} = \frac{1}{Q_o} + \frac{K_L C_e}{Q_o} \quad [2.8]$$

Where:

- C_e - is adsorbate concentration (ppm) at equilibrium.
- Q_e - is adsorbent amount at equilibrium.
- K_L - is equilibrium adsorption constant in accordance to affinity of the binding sites and energy of adsorption (L/mg).
- Q_o - is adsorbent amount at equilibrium for complete monolayer (mg/g).

K_L and Q_o values are calculated from the intercept and gradient of a straight-line graph of $\frac{C_e}{Q_e}$ against C_e .

The favorability of a sorption system is indicated by the dimensionless constant separation factor R_L . The adsorption nature is unfavorable if $R_L > 1$, linear if $R_L = 1$, irreversible if $R_L = 0$ and favorable if $0 < R_L < 1$ (Meroufel et al., 2013).

2.8.2 Freundlich Adsorption Isotherm

This technique assumes that Surface roughness, inhomogeneity and adsorbate-adsorbate interactions are uniform. It is based on an empirical equation that reflects a variation of energy with the adsorbed amount (Diour et al., 2014). The isotherm is valid for a heterogeneous surface that does not distribute heat for the adsorption process equally all over the surface of catalyst (Gulipalli et al., 2011).

Freundlich isotherm linear form is represented by equation (2.9) below:

$$\log Q_e = \log K_F + \frac{1}{n} \log C_e \text{-----}[2.9]$$

Where:

K_F and $\frac{1}{n}$ [adsorption intensity) are the Freundlich equilibrium coefficients.

A graph of $\log Q_e$ a $\log C_e$ results in a straight line with intercept $\log K_F$ and slope $\frac{1}{n}$. Low $\frac{1}{n}$ values show a large change in effectiveness over different equilibrium concentrations while larger K_F value indicates good adsorption efficiency for a particular adsorbent. The K_F constant which approximately indicates the adsorption capacity, while $\frac{1}{n}$ indicates the adsorption strength of a adsorption process and can be explained as shown below.

$\frac{1}{n} > 1$ - explains a physisorption process

$\frac{1}{n} < 1$ -explains a chemisorption process

2.9 Kinetic Studies

The rate determining steps and possible rates of a reaction can be illustrated using the kinetics models also called the time-concentration data. The kinetics of a adsorption system was demonstrated by either the pseudo-first-order or the pseudo-second-order models.

2.9.1 Pseudo First Order Model

The Lagergren pseudo first order model is given by the equation (2.10): $\log[qe - qt] = \log qe - \frac{k_1 t}{2.303}$ [2.10]

$$\log[qe - qt] = \log qe - \frac{k_1 t}{2.303} \quad [2.10]$$

2.303

Where

- qe - is adsorbed amount at equilibrium (mg/g)
- qt - is quantity absorbed at time t (mg/g)
- k_1 - is rate constant for the pseudo-first-order sorption (min^{-1})

Negative slope linear graph will be obtained from a straight line graph of $\log(qe - qt)$ against t . the graph is plotted at different concentrations, k_1 and qe values will be calculated from the gradient and intercept from the equation of the line respectively (Xie et al., 2011).

2.9.2 Pseudo Second Order Model

Pseudo second order kinetic model is shown below by equation (2.11):

$$\frac{t}{qt} = \frac{1}{k_2 qe} + \frac{t}{qe} \quad [2.11]$$

Where:

- k_2 - is rate constant for pseudo-second-order kinetic equation (g/mg min^{-1})
- qe - is the maximum adsorption capacity (mg/g)
- qt - is the amount (mg/g) of adsorption at time t .

A linear graph of $\frac{t}{qt}$ against t will be plotted and the qe and k_2 can be obtained from qt ,

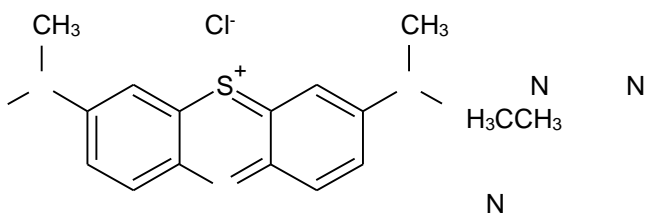
the gradient and intercepts (Xie et al., 2011).

2.10 Organic pollutant literature

This project is mainly sided with the degradation of organic dyes produced as waste effluent from industries by the photocatalytic technology. Methylene blue (C₁₆H₁₈ClN₃S) (MB) a synthetic dye utilized by different industries end up in the sewer systems of the industries. The trade names for methylene blue are Urelene blue, Proveblue and Provable. Methylene blue when ingested by humans have adverse effects such as nuisance, vomiting, high blood pressure, red blood cell interruption and serotonin. Henceforth due to these effects of methylene blue on human healthy, the compound has to be removed or degraded from waste water released by industries before it can be consumed by humans.

These synthetic organic dyes are commonly used in the clothing industry, shoe making industry, pulp and paper industry, food sciences, medical, agricultural and photoelectrochemical cells sector. The methylene blue structural formular is shown below.

Structure methyl blue as an organic dye



Chapter 3

9. pH meter

3.0 Materials and Methodology

3.1 Reagents and Apparatus

1. polytetrafluoroethylene-equipped stainless-steel autoclave,
2. Transmission electron microscope,
3. UV/ Vis spectrophotometer,
4. FTIR spectrophotometer
5. Incubation chamber
6. Centrifuge
7. magnetic stirrer
8. UV irradiation chamber

3.2 Synthesis of Carbon Quantum dots

1. Lemons,
2. Ethanol,
3. Deionized water,
4. Dichloromethane,
5. methyl blue
6. hydrous zinc nitrate
7. potassium hydroxide
8. hydrochloric acid
9. sodium hydroxide

Lemons were obtained from Bindura supermarket, washed using distilled water and extracted pulp-free lemon juice. Three mixtures of 24 milliliters of pulp-free lemon juice and 180 milliliters of ethanol were placed in three separately sealed glass bottles labelled 2, 4 and 6. The glass bottles were then put into an autoclave made of stainless steel and polytetrafluoroethylene, where carbonization of the mixtures occurred for 2 hours for the first bottle and 4 and 6 hours for bottle labelled 4 and 6 respectively at a continuous 120 °C and 15psi.

The brown colored solutions were obtained after carbonization reaction and the bottles were allowed cool to ambient temperature. Then dichloromethane was added in excess into each bottle to remove the unreacted organic molecules from the dark brown solution, and this process was repeated two to three times (He et al., 2018). The washed brown solutions were separated by centrifugation at 3500 rpm for 20 minutes to separate huge particles and obtain CQDs.

3.3 Synthesis of Zinc oxide

Zinc oxide nanoparticles were made utilizing a direct precipitation approach with potassium hydroxide as a precursor (Kaenphakdee et al., 2020). Separately, aqueous solutions of 0.2M Zinc Nitrate and 0.4M Potassium Hydroxide (KOH) was made in 500ml deionized water. The potassium hydroxide solution was pipetted into the zinc nitrate solution while stirring with magnetic stirrer, and a white precipitate was observed. The resultant solution was filtered, and the white precipitate was centrifuged for 15 minutes at 4500 rpm. After centrifugation the white

product was cleaned with distilled water twice and once with ethanol. In a muffle furnace, the resulting product was calcined for 3 hours at 500 °C.

3.4 Synthesis of CQDs/ Zinc Oxide Composite

The ZnO/CQDs composite was formed utilizing incubation technique (chu et al., 2019). ZnO formulated by the precipitation technique was mixed with CQDs pre-synthesized by hydrothermal approach and incubated at 30°C for 15 hours. Three sets of photocatalyst were made and named after the reaction time to which the CQDs were prepared. To each set 5g of ZnO was mixed with 20ml of CQDs paste. The main functional groups found on the carbon quantum dots such as –OH, –C=O and –COOH, bond to the ZnO by electronic interactions, The composite photocatalyst were named

1. ZnO/CQDs2
2. ZnO/CQDs4
3. ZnO/CQDs6

3.5 Preparation of water polluted with organic pollutants

The main organic pollutants in this case study are organic dyes mainly studying methyl blue degradation. 0.1g of solid methyl blue was dissolved in deionized water to make 100mg/L solution. 20mg/L solution of methyl blue was prepared by transferring 200 ml of 100mg/l into 1-liter volumetric flask and filled mark using distilled water. Serial dilutions were prepared from 5mg/l to 20mg/l and a calibration curve of methyl blue was plotted.

3.6 Characterization Methods

3.6.1 UV/ Vis spectrophotometer Analysis

A UV-Vis absorption spectra was measured by scanning on a UV-Vis spectrophotometer (Specord200) (He et al., 2018). The CQDs were dissolved in 20ml of distilled water and placed the solution in samples cells that have been cleaned with the solution containing the CQDs. The nanoparticles were synthesized under different condition that is varying the reaction time and measured their absorbance between 200nm to 400nm. .

3.6.2 FT-IR Spectrophotometer Analysis

Fourier Transform Infrared (FT-IR) (Shimadzu FT-IR 8400S, Japan) spectrophotometers was used to analyse the chemical bonds between the atoms in the CQDs.

3.6.3 Transmission Electron Microscope

By using a transmission electron microscope (JEM 2100, Japan) running at 300 KV, the morphology and microstructures of CQDs made from lemon juice were examined (He et al., 2018). Dropping the CQDs solution onto an ultrathin carbon film-coated copper grid with a mesh size of 300 prepared the CQDS for investigation on a TEM. The findings on the TEM were documented and recorded for further discussion

3.7 The pH_{zpc} determination

The pH displacement method was used to calculate pH_{zpc}.

3.8 Optimization parameter studies

Multiple trials were carried out to explore performance of the synthesized photocatalyst under different conditions. For this the photocatalyst ZnO/CQDs₆ was used. To observe the effect of contact time, samples were collected at 20 min intervals for 2 hrs. using the optimum dosage of 1.6g and changes in the concentration of methyl blue were measured. The effect of photocatalyst dose on the adsorption were observed by adding different amounts of the photocatalyst were added into separate 20ml of methyl blue contaminated water. The reaction was set for 1 hr., and pollutant concentration changes were measured. The effect solution pH was measured by changing pH at 2, 4, 6, 8, 10 and 12 at an optimum dosage of the photocatalyst. pH was varied by using 0.01M NaOH and or 0.01M HCl. Changes in the pollutant concentration was measured. The effect of temperature was observed by changing solution temperature between 20°C to 60°C using optimum photocatalyst dose. The effect of different catalyst composites was done by using ZnO/CQDs₂, ZnO/CQDs₄, ZnO/CQDs₆ and the results of the one with the highest efficiency was recorded.

3.9 Photocatalytic Degradation Of methylene blue

The three different photocatalyst composites were used for the degradation process. 1.6g of each catalyst was placed in separate beakers containing 20 mL of 20mg/l methyl blue solution and using a magnetic stirrer the mixtures were stirred for 60 minutes to attain adsorption–desorption equilibrium. The photocatalytic degradation process conditions were as follows:

1. Time: 2hrs
2. Dosage; 1.6g

3. Ph range: 6-8 and this process was done in a beaker surrounded with UV-lights. After two hours the aliquots of the photodegraded solutions were collected, centrifuged for 5 minutes at 1000 rpm and the calibration curve spectra of MB standards were recorded with UV-Vis spectrophotometer in order to determine % removal of the pollutant from waste water.

3.10 Data treatment methods

3.10 Removal capacity and adsorption capacity

Adsorption capacity, q_e , was calculated using the equation below:

$$Q_e = \frac{C_i - C_e}{m} \times V \text{-----(3.1)}$$

Where:

- C_i - is initial methyl blue concentration
- C_e - is methyl blue concentration at equilibrium
- V - is the volume of the solution
- m - is the weight of the photocatalyst

The removal capacity was calculated using the equation below

$$\%D = \frac{C_i - C_f}{C_i} \times 100 \text{-----(3.2)}$$

$C(i)$

Where:

- C_i - is initial concentration
- C_f – is final concentration

3.11 Model fitting analysis

3.11.1 Adsorption Isotherms

To calculate maximum adsorption capacity and intensity of methyl blue on ZnO/CQDs6 photocatalyst, Langmuir and Freundlich isotherms were used to analyse the thesis data. Langmuir,

is given by equation (2.8). The values of KL and Qo are obtained from the intercept and slope of the graph of Ce/qe vs Ce respectively. Freundlich is given by equation (2.9)

3.11.2 Kinetic Studies

To study the time-concentration data which controls the process, pseudo first order and pseudo second order were used and validity of these models were verified using equation [2.10] and equation [2.11] respectively. A graph of log (qe-qt) against t provided the k1 and qe values for the pseudo first order modelling and k2 and qe values were obtained from gradient and intercept of a graph of $\frac{t}{q_e - q_t}$ against t for pseudo second order.

q_e

3.11.3 Thermodynamics studies

To evaluate ΔH° and ΔS° the vant's equation below was used;

$$\ln kd = \frac{\Delta H^\circ}{RT} + \frac{\Delta S^\circ}{R} \text{-----} (3.3)$$

Where

$$kd = \frac{C_{Ac}}{C_e} \text{-----} (3.4)$$

To find Gibbs free energy ΔG , the below equation was used;

$$\Delta G^\circ = -RT \ln Kd \text{-----} (3.5)$$

Where:

- R- is gas constant
- T- is experimental temperature,
- K_d– is distribution coefficient.

Chapter 4

4.0 Results and discussion

4.1 Physicochemical analysis

4.1.1 Synthesis

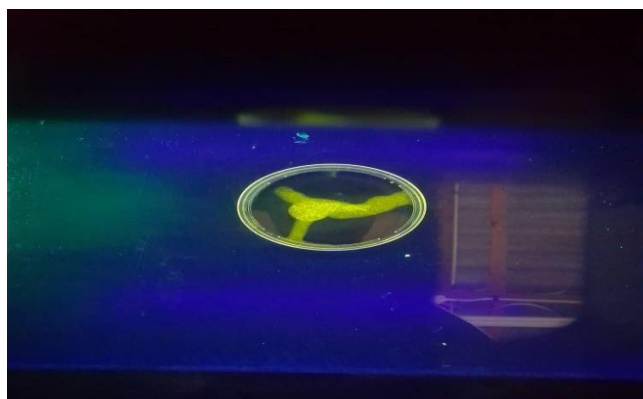
After extracting the pulp free lemon juice, 24ml of the juice was dissolved in 180ml of ethanol and autoclaved at 120 °C and a pressure of 15 psi (1.035 bars) for 2,4, and 6hrs separately. A brown solution was obtained and bubbles were observed on reacting the solution with dichloromethane removing the unreacted organic compounds and two phases were obtained one containing the brown solution and the other was a white paste. The two phases were separated by the by centrifuge for 20 minutes at rotating speed of 3500 rpm. Carbon quantum dots were then obtained. The *figure 4.1* below shows the appearance of CQDs in daylight, UV radiation and fluorescence radiation.



(a)



(b)



[c]

Figure 4.1 showing result of CQDs when observed in (a) daylight (b)UV radiation (c)Fluorescence radiation

The brown color is observed when in daylight but after exposure to UV radiation the CQDS showed a blue color and greenish color of carbon quantum dots when exposed to fluorescence irradiation. The color observed is evident of photoluminescence characteristics of the carbon quantum dots formulated from the citrus lemon juice.

4.1.2 pH_{pzc} analysis

After measuring pH using a pH meter, the pH of the photocatalysts were recorded in table 4.1 below. The photocatalyst differs in the carbonization time taken for the CQDs synthesis. To evaluate if the surfaces of the synthesized photocatalyst is negatively charged or positively charged, the pH_{pzc} were measured. The results obtained showed that pH_{pzc} of ZnO/CQDs lied ranges from 8 to 9 for all the catalyst that were tested. However, as the solution pH increases the pH_{pzc} of the photocatalyst also reduces to zero or becomes less positive and the results of photooxidation of the methylene blue will be enhanced. The reduced photooxidation efficiency of methyl blue in acidic conditions is because the presents of H^+ ions compete with MB cationic species that absorb to the photocatalyst surface.

Table 4.1 physical characteristics of the photocatalyst

Photocatalyst	Ph	pH _{pzc}
ZnO/CQDs 2	6.7	8
ZnO/CQDs 4	7.2	8.3
ZnO/CQDs 6	7.6	9

4.2 FTIR spectra for the analysis for the surface functional groups of the ZnO/CQDs

The FTIR spectra of ZnO/CQDs6 was illustrated in figure 4.2 and it showed several distinct vibrational bands which explains the various functional groups found in the photocatalyst composite. The strong bands observed between 600 to 900 on the FTIR spectra indicates the ZnO stretching vibrations. The vibrational bands between 1100 to 1500 is evident that they are C-O species either of the carboxylic group or the tertiary alcohol in the CQDs of which were used to form the composite photocatalyst. The band observed at 1699.33 is evident of the C=C stretching vibrations of the sp^2 hybridized aromatics structures in the carbon quantum dots.

The spectrum shows a band at 2139,15 which indicates the presents of the alkynes group in the carbonized CQDs. The vibrational bands observed between the 3000-4000 indicated O-H stretching of the chemically absorbed water molecules by ZnO/CQDs photocatalyst.

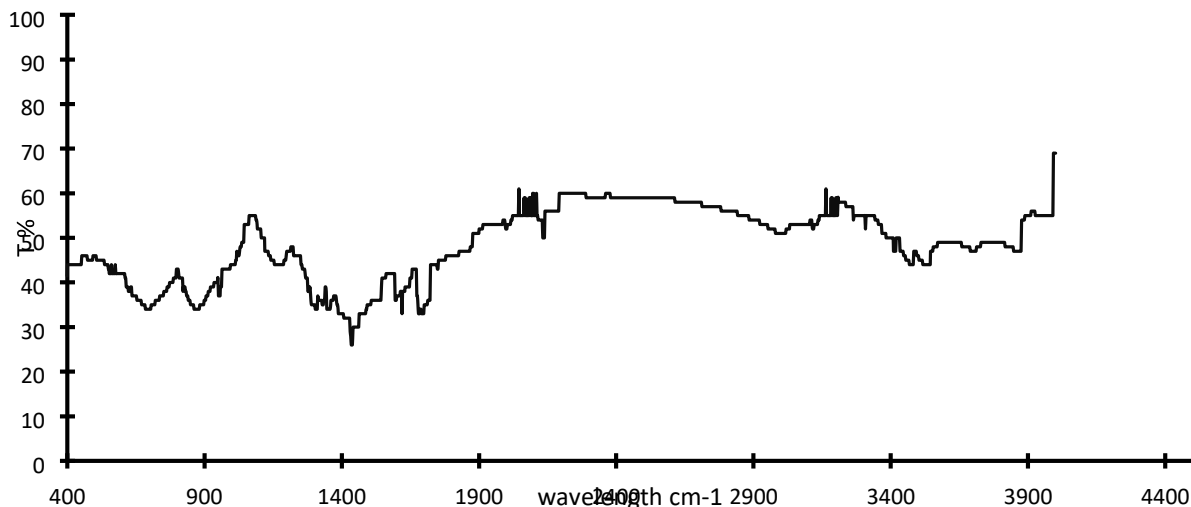


Figure 4.2 showing the FTIR spectra of the three synthesized CQDs

4.3 photocatalytic degradation of methyl blue

Photocatalytic activity experiments with different photocatalysts namely ZnO/CQDs 2, ZnO/CQDs 4, ZnO/CQDs 6 which differ in the reaction time of synthesis of CQDs. The experiments were carried out with 1.6g mass of the photocatalyst. The photocatalytic efficiency is illustrated in *fig 4.3* below. The different photocatalyst had 45.30%, 76.40%, 95.04% degradation for ZnO/CQDs 2, ZnO/CQDs 4, ZnO/CQDs 6 respectively when observed after 80 minutes of degradation process.

The efficiency of the degradation process with the different photocatalyst indicates the different abilities of the CQDs in the reducing the reflective characters of ZnO to light absorption, and enhancing formation of hydroxy radical for the degradation process. Also, the results obtained for the low degradation percentage could be as a result of BET mismatch of the photocatalyst surface which affects the way methylene blue adsorbs to the photocatalyst surface, the contact time and rate of the recombination of the electron-hole pairs. The surface area of the photocatalysts is the main factor which gives information to the number of organic contaminants that are adsorbed to enhance the photooxidation process (Chen et al., 2004). On the other hand, the light harvesting power of ZnO/CQDs6 was far much greater than that ZnO/CQDs2 and, ZnO/CQDs4 hence the difference in % degradation.

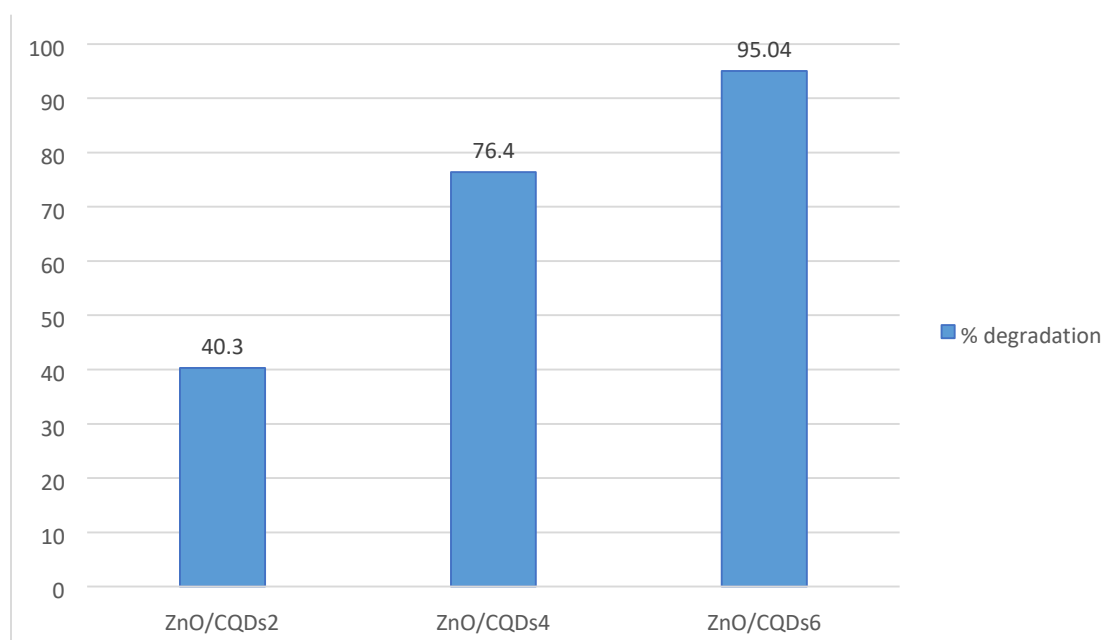


Figure 4.3 showing the % degradation of methyl blue with different catalysts

4.4 Optimization parameters

4.4.1 effect of temperature

The experiment was carried out using 1.6g of ZnO/CQDs6 composite photocatalyst varying the temperature from 20-50 °C. 20ml of 20mg/l methyl blue was used for photodegradation. The data showing temperature effect on photocatalysis is illustrated in fig 4.4. 36.5 % degradation obtained at 20 °C as a result of, slow desorption of the products formed which reduces the rate reaction at low temperatures. At these temperatures there is slower rate of photo-degradation on ZnO/CQDs6 surface and the adsorption of the reactants. As the temperatures increases from 25°C , 30°C, 35°C , 40 °C, 45°C, the percentage of degradation process were 64.9 %, 80%, 81.5%,77.9%,75% respectively. The % degradation increases because the rate of adsorption of reactants increases and rate at which products are removed from the ZnO/CQDs6 also increases. In addition, increase in temperature positively favors the rate of MB adsorption to ZnO/CQDs6 for spontaneous endothermic reaction.

In comparison, temperature above 35°C, the rate at which the MB adsorbed to ZnO/CQDs surface will be very low and have a tendency of limiting the reaction (Mehrotra et al., 2005) and the limiting step will be the adsorption of the pollutant (methyl blue) on ZnO/CQDs and that is the reason why there is drop on rate of degradation process. The reduced capability of adsorption that

is encountered with organic and oxygen substrates at temperatures above 35°C decreases the rate constant (Zhou et al., 2003). Therefore, the optimum temperature obtained in this study was between 30°C and 35°C

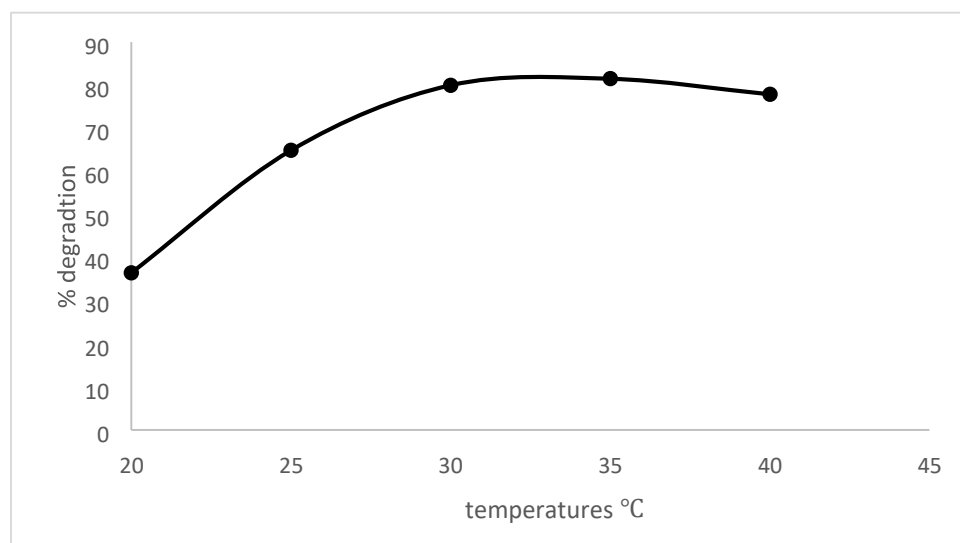


Figure 4.4 effect of temperature on the photodegradation of methyl blue

4.4.2 Effect of pH

To study pH variation effect on rate of degradation the pH was adjusted using NaOH and HCl. The results illustrated in *fig 4.5* at pH 2, 4, 6, 8, 10, 12 the % degradation were 18.4, 34.5, 57.9, 68.2, 68.2, and 55.8 respectively. At low pH values i.e., $\text{pH} \leq 5$, % degradation of the methylene blue is low because the proton are highly concentrated in that region of the pH meter which competes with the cationic dye for the adsorption sites, giving a low rate of degradation. The pH ranges from 6 – 8 are the favorable ranges as the photocatalytic degradation of methyl blue because at this pH range there are few positive holes and hydroxy radicals will be predominant resulting in the high rate of degradation. In acidic conditions are the most prevalent oxidation species are the positive holes while in alkaline and neutral regions the hydroxy radicals are the most prevalent species for photooxidation process (Khairnar et al., 2018).

Moreover, in alkaline solutions i.e., $\text{pH} \geq 9$, hydroxyl ions will be excess and neutralizes acidic products formed during the photooxidation process. thus, at pH above 9 the rate of degradation process drops significantly. Also, at higher pH the methylene blue dye structure is also neutralized and become stable to degradation to the extent that even after light irradiates the solution containing MB and ZnO/CQDs6 the hydroxy radicals produced does not have any impact on the

dye (Tsui and Chu, 2001). In conclusion, at higher pH the changes that happens to the dye structure limits the rate of reaction.

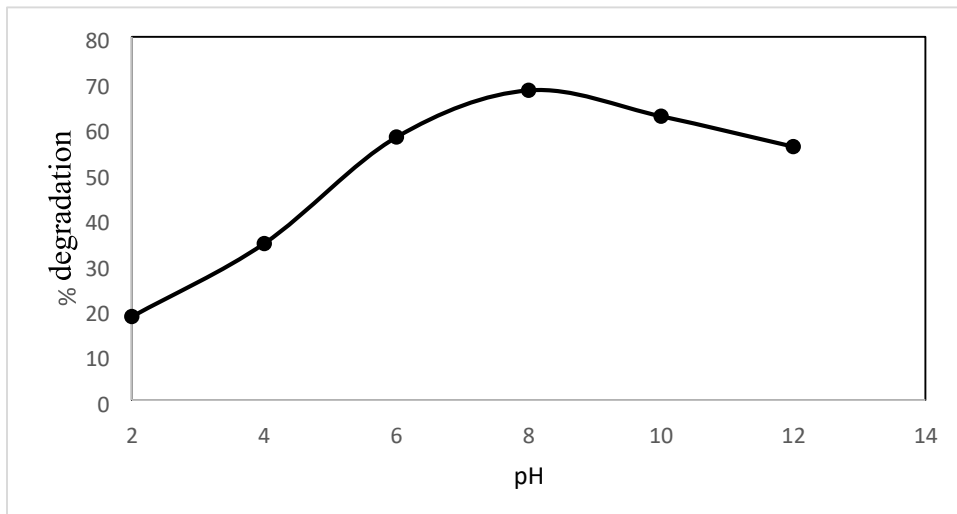


Figure 4.5 effect of temperature on the photodegradation of methyl blue

4.4.3 Effect of adsorption time

The influence of time on photo-degradation efficiency of methyl blue with ZnO/CQDs was examined with 1.6g mass of photocatalyst and the initial concentration of methyl blue solution of 20 mg/l. The data obtained was recorded in *fig 4.6* illustrates a sharp increase from 0 to 75% degradation from 0 to 60 minutes. The trend observed on removal of methyl blue with respect to time is because of availability of more adsorption sites for methyl blue to be adsorbed. The degradation rate is a function of free adsorption sites (Ayawei et al., 2017).

At 80 minutes there was a slight increase to 85% degradation and then the rate of degradation became constant. The slight increase in % degradation shows the onset of adsorption site limitation until it reaches the equilibrium where now the rate of adsorption of MB and the desorption of carbon dioxide and water are equal.

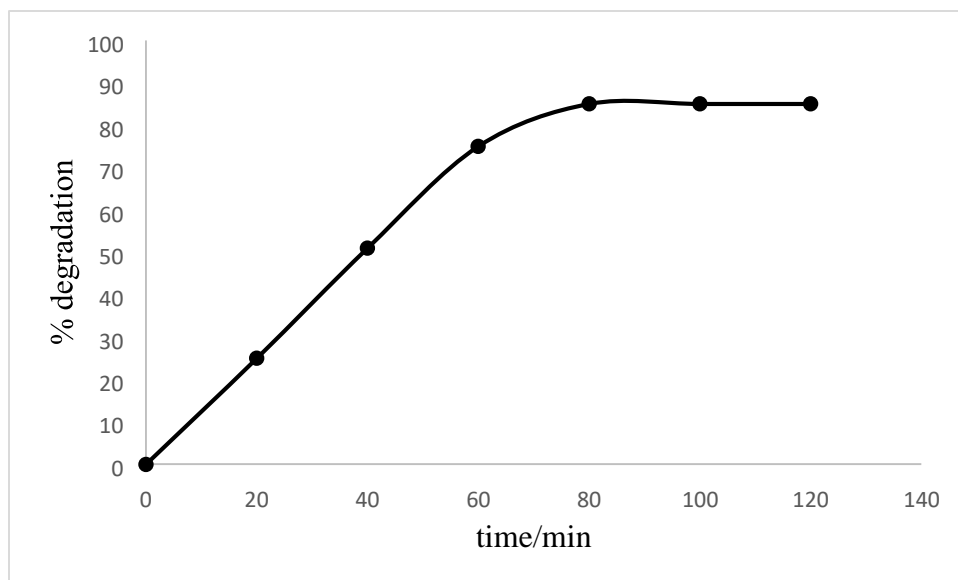


Figure 4.6 effects of time on the photodegradation of methyl blue

4.4.4 Effect of photocatalyst dosage

The photocatalyst dose affect the photo-oxidation process in a good and bad way (Wei et al., 1991). According to the results obtained in *fig 4.7*, the initial degradation rates followed a direct proportionality with respect to the catalyst dose which is evident of a heterogeneous regime of ZnO/CQDs6 photocatalyst. The maximum degradation efficiency of 75% was obtained when the dosage was at 1.6g. dosage at 2g and 2.4g gave a degradation efficiency of 72% and 65% respectively

As the photocatalyst dose increases, the light absorbing power also increases and the rate of the reaction also increases (Muruganandham, Swaminathan., 2006) and also it increases the adsorption sites of the photocatalyst. However, higher dosages beyond the optimum dose causes surface area loss due to clotting of the photocatalyst particles and increase solution cloudiness thereby decreasing the penetrating power on the photon flux in the reactor (Gogate and Pandit, 2004). This explains the decrease in the photodegradation process.

Henceforth, an optimum amount of ZnO/CQDs composite used in this study for the photocatalytic degradation process was 1,6g in 20mg/l of methyl blue so as to make maximum light absorption and get maximum photodegradation at reduce cost.

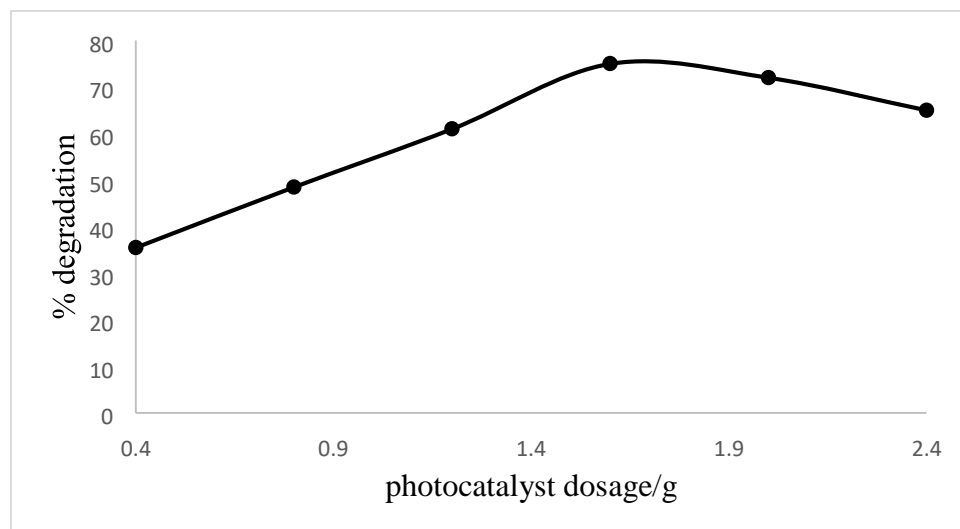


Figure 4.7 effects of catalyst dosage on the photodegradation of methyl blue

4.5 Model fitting analysis

4.5.1 Adsorption isotherms

The adsorption isotherm experimental data two parameters namely the Freundlich described by the equation (2.9), and Langmuir describes by the equation (2.8) were used. The Freundlich equilibrium isotherm equation describes the adsorption of MB which passes through multilayers on the catalyst surface. The technique is rooted on adsorption of substrates onto heterogeneous layers by physisorption with uniform distribution of energy. The Langmuir model gives an account on adsorption on the monolayer outer surface of ZnO/CQDs (Rangabhashiyam et al., 2014). The approach also accounts for the equilibrium distribution of the adsorbate between the solid and liquid phases and is affected by increase in temperature.

The results of the study are illustrated in figure 4.8[a] and [b], table 4.2. The degradation of methylene blue with ZnO/CQDs6 favored Langmuir adsorption isotherm to a significant degree than Freundlich isotherm. This was demonstrated by the correlation coefficient obtained in Table 4.2. The correlation coefficient for Langmuir isotherm for methyl blue degradation was $R^2 - 0.8259$ and Freundlich correlation coefficient was $R^2-0.1577$. The high correlation coefficient value for Langmuir isotherm over Freundlich isotherm simply indicate that the experiment was conducted using the Langmuir isotherm model's assuming:

1. Adsorption does not go beyond the monolayer,
2. Adsorption on the adsorbent occurs specific sites,

3. As the contaminant fills a site, adsorption in that site can occur again.
4. the energy of adsorption is independent on the rate of occupation on an adsorbent's active centers and is the same;
5. The photocatalyst surface have fixed capacity for the contaminants.
6. all sites are equal and energetically the same.
7. the adsorbent is anatomically homogeneous
8. The adsorbed molecules have no effect on the neighboring sites (Langmuir, 1918).

Adsorption capacity values were 0.76 and 1.01 for Langmuir and Freundlich isotherms respectively. The higher adsorption value of k for Freundlich is also evidence of high adsorption capability. $1/n$ value obtained was 0.051 which is evidence that the experiment favors physisorption compared to chemisorption.

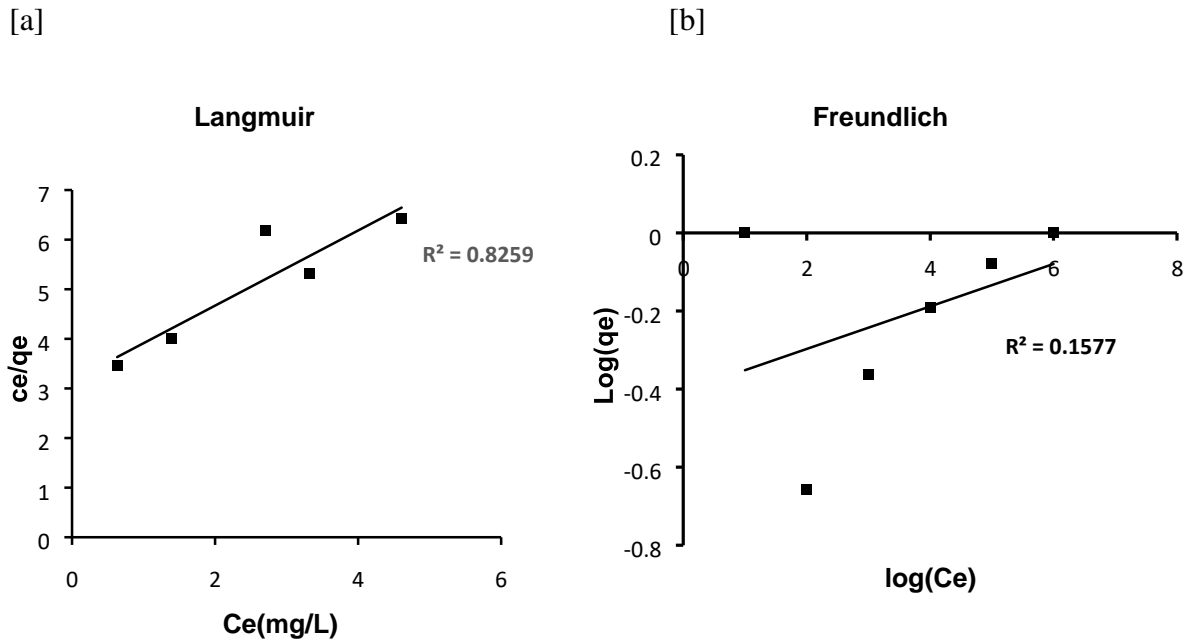


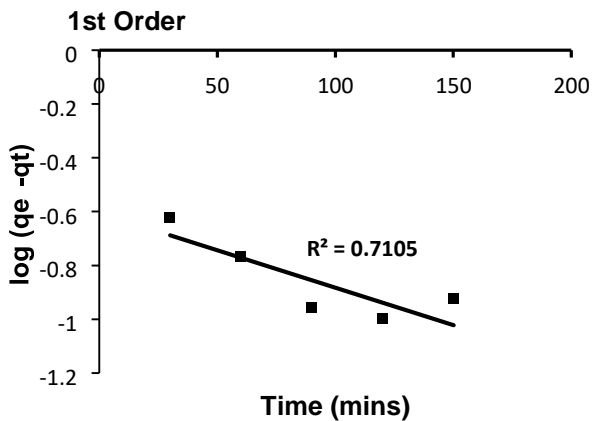
Figure 4.8 data analysis for [a] Langmuir and [b] Freundlich isotherms

4.5.2 Reaction kinetics (pseudo)

Time–concentration data used to study the kinetics of the photo-degradation of methyl blue with ZnO/CQDS6. This data was calculated using the pseudo-first-order equation (2.10) and pseudosecond-order equation (2.11). The pseudo- first- order kinetic model explains the adsorption of solid–liquid phases that relies upon adsorption capacity of solids (Lagergren, 1898). The pseudosecond-order kinetic model works with a hypothesis which states that “adsorption rate follows second order reaction”. This technique assumes that one of the contaminant fragments will be adsorbed onto two adsorption sites of ZnO/CQDs.

The photo-degradation of methyl blue by ZnO/CQDs6 catalyst followed pseudo-first-order as evidenced by the linear regression coefficients obtained in *fig4.9(a and b) table (4.2)*. The coefficients were 0.7105 min^{-1} and $0.363 \text{ mg g}^{-1} \text{ min}^{-1}$ for pseudo-first-order and pseudo second order respectively. The higher linear regression coefficient indicates that the reaction favors pseudo-first-order. Moreover, the rate constants for the pseudo first order and pseudo second order were 1.98 per minute and 0.23 mg/min. The rate constants also is clear evident that the reaction favors the pseudo-first-order. The adsorption capacity for pseudo first order and pseudo second order recorded in table (4.2) were 0.279 and 33.21 respectively. With the adsorption capacity data, it can be noticed the reaction is first order.

[a]



[b]

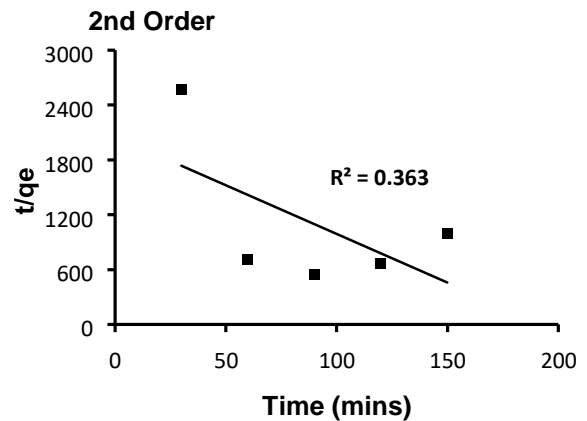


Figure 4.9 data on reaction kinetic

Table 4.2 adsorption isotherm parameters and reaction kinetics parameters

	<i>Linear Equation</i>	<i>Coefficients</i>	<i>R₂</i>
Isotherm model			
Langmuir Isotherm	$y = 0.7568x + 3.1564$	$q_m = 0.94 \text{ mg g}^{-1}$	0.8259
		$K_L = 0.76 \text{ L mg}^{-1}$	
Freundlich Isotherm	$y = 0.0545x - 0.4061$	$1/n = 0.054 \text{ L g}^{-1}$	0.1577
		$K_F = 1.01 \text{ mg g}^{-1}$	
Reaction Kinetics			
Pseudo First-Order	$y = -0.0028x - 0.6049$	$K_1 = 1.98 \text{ min}^{-1}$	0.7105
		$Q_e = 0.279 \text{ mg g}^{-1}$	
Pseudo Second-Order	$y = -10.649x + 2054.5$	$K_2 = 0.23 \text{ mg g}^{-1} \text{ min}^{-1}$	0.363
		$Q_e^2 = 33.21 \text{ mg g}^{-1} \text{ min}^{-1}$	

4.5.3 Thermodynamic study

The thermodynamic studies for the photocatalytic oxidation of methyl blue with ZnO/CQDs are presented in figure (4.10) table (4.3). The Gibbs free energy values for the degradation of methyl blue were recorded at different temperatures and negative ΔG values explains a reaction that is feasible and spontaneous. Also, negative ΔG values obtained at 298 K was $-2.19 \text{ KJ mol}^{-1}$, at 303 K was $-0.47 \text{ KJ mol}^{-1}$ and at 313K was 1.10 KJ mol^{-1} . From the results obtained the most spontaneous reaction was observed at 298K which was $-2.19 \text{ KJ mol}^{-1}$ followed by at 303K which was $-0.47 \text{ KJ mol}^{-1}$ and then lastly at 313K which was 1.10 KJ mol^{-1} . The ΔG free energy becomes less negative with increase in temperature; therefore, the reaction becomes less spontaneous with the increase in temperature and at 313 the reaction was non-spontaneous indicated by the positive ΔG .

The positive enthalpy change of 0.21 KJ mol^{-1} of reaction indicates that degradation of the contaminant (methyl blue) with ZnO/CQDs nanocomposite is endothermic and endergonic. The entropy for photooxidation of methyl blue was $65118.5 \text{ J k}^{-1} \text{ mol}^{-1}$ indication that the reaction is highly disordered or random. The positive entropy also is evidence that the reaction is spontaneous.

Henceforth, the reaction thermodynamic studies of this study overall states that the reaction was spontaneous, endothermic and highly disordered.

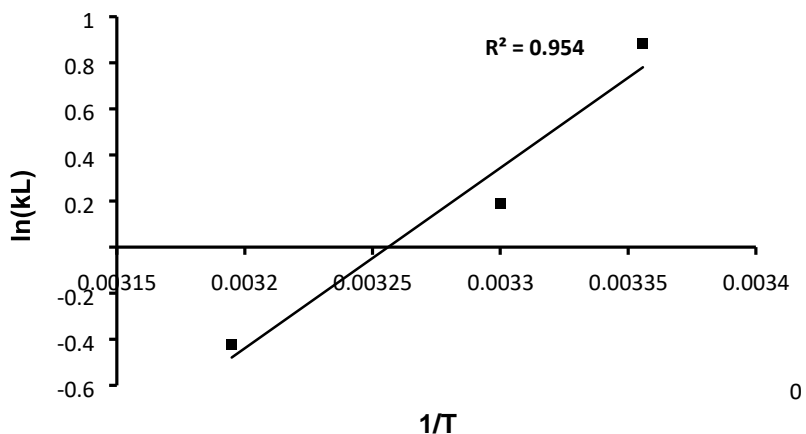


Figure 4.10 data showing thermodynamic parameters

Table 2.3 thermodynamic parameters

	ΔH (Kj mol ⁻¹)	ΔS (J k ⁻¹ mol ⁻¹)	ΔG (KJ mol ⁻¹)		
			298K	303K	313K
ZnO/CQDs6	0.21	65118.57	-2.19	-0.47	1.10

4.6 Comparative study

The degradation activities of methyl blue with different photocatalysts reported in recent year are briefly in Table 4.4. Comparing the current study results with other reported photocatalysts results, the ZnO/CQDs prepared possessed excellent photo-degradation of methyl blue. Moreover, the photocatalyst ZnO/CQDs can be used in preference to other traditional semiconductor photocatalyst in the photocatalytic technology that involves the degradation of methylene blue MB.

Table 4.4 the photocatalytic activity of ZnO/CQDs comparison with other different photocatalysts for methy blue degradation in recent years

photocatalyst	% degradation	reference
MnTiO3 nanoparticles	70 - 75%	Alkaykh et al., 2020
TiO2/AC	98%	Asim et al., 2014
TiO2/PANi	84.7%	Asim et al., 2014
ZnO/GPET	83.6%	Rong et al., 2022
ZnO/CQDs	95.04%	Current study

4.7 Photodegradation mechanism and reaction scheme

The possible photocatalytic degradation mechanism for the degradation of methyl blue is explained in *chapter 2 section 2.3.1 and figure 2.1*. However, the reaction scheme for the photodegradation of methyl blue to water and carbon dioxide using the catalyst ZnO/CQDs6 composite photocatalyst is shown in fig 4.10 below

Chapter 5

5.1 Conclusion

In summary, ZnO produced by the precipitation method and CQDs produced by hydrothermal synthesis from lemon juice were used to formulate a composite photocatalyst by the incubation method. The composite photocatalyst was utilized in the photodegradation of the organic contaminant methyl blue. The catalyst ZnO/CQDs6 was capable of degrading methyl blue from the waste water with a high degradation efficiency 95.04. The photocatalyst was assessed using the FTIR spectroscopy and the methyl blue calibration curve was plotted utilizing the UV- Vis spectroscopy. Based on pH, temperature, photocatalyst dose, and contact time, methyl blue from waste water degraded at a different pace depending on changes of these factors. The results of the adsorption investigations demonstrated that the degradation of the methyl blue employed the Langmuir adsorption isotherm, in which physisorption happened via the pseudo-first-order process. The reaction was spontaneous and endothermic, according to thermodynamic analyses. According to the results of this thesis, the ZnO/CQDs catalyst is a promising photocatalyst that may be employed extensively to degrade organic contaminants in wastewater.

5.2 Recommendations

Future research should include:

- More research on nanotech carbon sources used to enhance the use of traditional semiconductor catalyst in decay of organic contaminants.
- Recycling of the photocatalyst and study its efficiency in decay of organic contaminants.
- Assessment on the BOD and COD of the disposed sludge after photocatalytic degradation process in order to reduce environmental pollution

References

- Meshram, S.P.; Adhyapak, P.V.; Pardeshi, S.K.; Mulla, I.S.; Amalnerkar, D.P. Sonochemically generated cerium doped ZnO nanorods for highly efficient photocatalytic dye degradation. *Powder Technol.* **2017**, 318, 120-127.
- Yibeltal, A.W.; Beyene, B.B.; Admassie, S.; Tadesse, A.M. MWCNTs/Ag-ZnO nanocomposite for efficient photocatalytic degradation of congo red. *Bull. Chem. Soc. Ethiop.* **2020**, 34, 55-66.
- Ding, H.; Yu, S.-B.; Wei, J.-S.; Xiong, H.-M. Full-color light-emitting carbon dots with a surface-state-controlled luminescence mechanism. *ACS nano* **2016**, 10, 484-491.
- Shen, J.; Zhu, Y.; Yang, X.; Li, C. Graphene quantum dots: emergent nanolights for bioimaging, sensors, catalysis and photovoltaic devices. *Chem. commun.* **2012**, 48, 3686-3699.
- Bozetine, H.; Meziane, S.; Aziri, S.; Berkane, N.; Allam, D.; Boudinar, S.; Hadjersi, T. Facile and green synthesis of a ZnO/CQDs/AgNPs ternary heterostructure photocatalyst: Study of the methylene blue dye photodegradation. *Bull. Mater. Sci.* **2021**, 44, 1-12.
- Djurišić, A.B.; Chen, X.; Leung, Y.H.; Ng, A.M.C. ZnO Nanostructures: Growth, Properties and Applications. *J. Mater. Chem.* 2012, 22, 6526–6535.
- Kumar, S.G.; Rao, K.S.R.K. Zinc Oxide Based Photocatalysis: Tailoring Surface-Bulk Structure and Related Interfacial Charge Carrier Dynamics for Better Environmental Applications. *RSC Adv.* 2015, 5, 3306–3351
- Li, Y.; Zhang, B.P.; Zhao, J.X.; Ge, Z.H.; Zhao, X.K.; Zou, L. ZnO/Carbon Quantum Dots Heterostructure with Enhanced Photocatalytic Properties. *Appl. Surf. Sci.* 2013, 279, 367–373
- Xu, X.; Ray, R.; Gu, Y.; Ploehn, H.J.; Gearheart, L.; Raker, K.; Scrivens, W.A. Electrophoretic analysis and purification of fluorescent single-walled carbon nanotube fragments. *J. Am. Chem. Soc.* **2004**, 126, 12736–12737.
- Muthulingam, S.; Lee, I.H.; Uthirakumar, P. Highly Efficient Degradation of Dyes by Carbon Quantum Dots/N-Doped Zinc Oxide (CQD/N-ZnO) Photocatalyst and Its Compatibility on Three Different Commercial Dyes under Daylight. *J. Colloid Interface Sci.* 2015, 455, 101–109.

Yu, H.; Zhao, Y.; Zhou, C.; Shang, L.; Peng, Y.; Cao, Y.; Wu, L.Z.; Tung, C.H.; Zhang, T. Carbon Quantum Dots/TiO₂ Composite for Efficient Photocatalytic Hydrogen Evolution. *J. Mater. Chem. A* 2014, 2, 3344–3351

Hallaj T, Amjadi M, Manzoori JL et al (2015) Chemiluminescence reaction of glucose-derived graphene quantum dots with hypochlorite, and its application to the determination of free chlorine. *Microchim Acta* 182(3–4):789–796

Dong Y, Shao J, Chen C et al (2012) Blue luminescent graphene quantum dots and graphene oxide prepared by tuning the carbonization degree of citric acid. *Carbon* 50(12):4738–4743

Wang, S.; Chen, Z.G.; Cole, I.; Li, Q. Structural evolution of graphene quantum dots during thermal decomposition of citric acid and the corresponding photoluminescence. *Carbon* **2015**, 82, 304–313.

V. Ramanan, S.K. Thiyagarajan, K. Raji, R. Suresh, R. Sekar, P. Ramamurthy, Outright green synthesis of fluorescent carbon dots from eutrophic algal blooms for in vitro imaging, *ACS Sustain. Chem. Eng.* 4 (2016) 4724–4731

Xu X, Ray R, Gu Y et al (2004) Electrophoretic analysis and purification of fluorescent singlewalled carbon nanotube fragments. *J Am Chem Soc* 126(40):12736–12737

Jia X, Li J, Wang E (2012) One-pot green synthesis of optically pH-sensitive carbon dots with upconversion luminescence. *Nanoscale* 4(18):5572–5575

Xu, M.; He, G.; Li, Z.; He, F.; Gao, F.; Su, Y.; Zhang, L.; Yang, Z.; Zhang, Y. A green heterogeneous synthesis of N-doped carbon dots and their photoluminescence applications in solid and aqueous states. *Nanoscale* **2014**, 6, 10307–10315. [CrossRef]

Wan, J.Y.; Yang, Z.; Liu, Z.G.; Wang, H.X. Ionic liquid-assisted thermal decomposition synthesis of carbon dots and graphene-like carbon sheets for optoelectronic application. *RSC Adv.* **2016**, 6, 61292–61300.

Lai, Q.; Zheng, J.; Tang, Z.; Bi, D.; Zhao, J.; Liang, Y. Optimal Configuration of N-Doped Carbon Defects in 2D Turbostratic Carbon Nanomesh for Advanced Oxygen Reduction Electrocatalysis. *Angew. Chem. Int. Ed.* **2020**, 59, 11999–12006.

Zou, J.; Lin, Y.; Wu, S.; Zhong, Y.; Yang, C. Molybdenum Dioxide Nanoparticles Anchored on Nitrogen-Doped Carbon Nanotubes as Oxidative Desulfurization Catalysts: Role of Electron Transfer in Activity and Reusability. *Adv. Funct. Mater.* **2021**, *31*, 2100442.

Sun, Y.P.; Zhou, B.; Lin, Y.; Wang, W.; Fernando, K.A.S.; Pathak, P.; Mezziani, M.J.; Harruff, B.A.; Wang, X.; Wang, H.; et al. Quantum-sized carbon dots for bright and colorful photoluminescence. *J. Am. Chem. Soc.* 2006, *128*, 7756–7757.

Reyes, D.; Camacho, M.; Camacho, M.; Mayorga, M.; Weathers, D.; Salamo, G.; Wang, Z.; Neogi, A. Laser ablated carbon nanodots for light emission. *Nanoscale Res. Lett.* 2016, *11*, 424.

Park, S.Y.; Lee, H.U.; Lee, Y.C.; Choi, S.; Cho, D.H.; Kim, H.S.; Bang, S.; Seo, S.; Lee, S.C.; Won, J.; et al. Eco-friendly carbon-nanodot-based fluorescent paints for advanced photocatalytic systems. *Sci. Rep.* **2015**, *5*, 12420.

Li, H.; He, X.; Liu, Y.; Huang, H.; Lian, S.; Lee, S.T.; Kang, Z. One-step ultrasonic synthesis of water-soluble carbon nanoparticles with excellent photoluminescent properties. *Carbon* **2011**, *49*, 605–609.

Tao, S.; Song, Y.; Zhu, S.; Shao, J.; Yang, B. A new type of polymer carbon dots with high quantum yield: From synthesis to investigation on fluorescence mechanism. *Polymer* **2017**, *116*, 472–478.

Lu, W.; Qin, X.; Liu, S.; Chang, G.; Zhang, Y.; Luo, Y.; Asiri, A.M.; Al-Youbi, A.O.; Sun, X. Economical, green synthesis of fluorescent carbon nanoparticles and their use as probes for sensitive and selective detection of mercury(II) ions. *Anal. Chem.* 2012, *84*, 5351–5357.

Ma, X.; Dong, Y.; Sun, H.; Chen, N. Highly fluorescent carbon dots from peanut shells as potential probes for copper ion: The optimization and analysis of the synthetic process. *Mater. Today Chem.* 2017, *5*, 1–10.

So, R.C.; Sanggo, J.E.; Jin, L.; Diaz, J.M.A.; Guerrero, R.A.; He, J. Gram-scale synthesis and kinetic study of bright carbon dots from citric acid and *Citrus japonica* via a microwave-assisted method. *ACS Omega* 2017, *2*, 5196–5208.

Yang, Y.; Liu, N.; Qiao, S.; Liu, R.; Huang, H.; Liu, Y. Silver modified carbon quantum dots for solvent-free selective oxidation of cyclohexane. *New J. Chem.* 2015, *39*, 2815–2821. [CrossRef] Liu,

M.; Xu, Y.; Niu, F.; Gooding, J.J.; Liu, J. Carbon quantum dots directly generated from electrochemical oxidation of graphite electrodes in alkaline alcohols and the applications for specific ferric ion detection and cell imaging. *Analyst* 2016, 141, 2657–2664.

Han, N.; Guo, X.Y.; Cheng, J.L.; Liu, P.Y.; Zhang, S.G.; Huang, S.P.; Rowles, M.R.; Fransaer, J.; Liu, S.M. Inhibiting in situ phase transition in Ruddlesden-Popper perovskite via tailoring bond hybridization and its application in oxygen permeation. *Matter* **2021**, 4, 1720–1734. [CrossRef]

Z. Shekarbeygi, N. Farhadian, S. Khani, S. Moradi, M. Shahlaei, The effects of rose pigments extracted by different methods on the optical properties of carbon quantum dots and its efficacy in the determination of Diazinon, *Microchem. J.* 158 (2020), 105232.

Q. Jiang, Y. jing, Y. Ni, R. Gao, P. Zhou., Potentiality of carbon quantum dots derived from chitin as a fluorescent sensor for detection of ClO⁻, *Microchem. J.* 157 (2020), 105111.

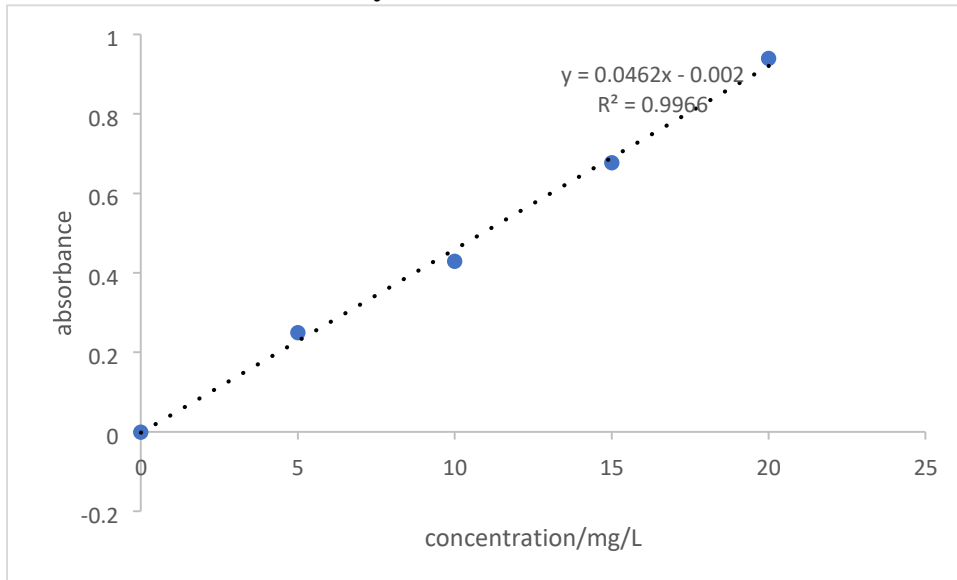
M. Misra, R. K. Gupta, A. K. Paul and M. Singla, *J. Power Sources*, 2015, 294, 580–587.

Liu, Y.; Fang, L.; Lu, H.; Li, Y.; Hu, C.; Yu, H. One-Pot Pyridine-Assisted Synthesis of VisibleLight-Driven Photocatalyst Ag/Ag₃PO₄. *Appl. Catal. B Environ.* 2012, 115, 245–252.

Abderrahim, N.; Djellabi, R.; Amor, H.B.; Fellah, I.; Giordana, A.; Cerrato, G.; Di Michele, A.; Bianchi, C.L. Sustainable Purification of Phosphoric Acid Contaminated with Cr(VI) by Ag/Ag₃PO₄ Coated Activated Carbon/Montmorillonite under UV and Solar Light: Materials Design and Photocatalytic Mechanism. *J. Environ. Chem. Eng.* **2022**, 10, 107870.

Xie, X., Hu, Q., Shi, X. and Wu, Z., (2011) Studies on the Kinetics and Mechanism of Thermal Decomposition of ZnAl-hydrotalcite-like Compounds. *ChemInform*.

**Appendix
Calibration curve of methyl blue**



Appendix 2 Adsorption isotherm data

Langmuir

volume(L)	mass(g)	Ci(mg/L)	Ce(mg/L)	Qe	Ce/qe
0.2	1.6	2	0.631	0.182533	3.456903
0.2	1.6	4	1.39	0.348	3.994253
0.2	1.6	6	2.71	0.438667	6.177812
0.2	1.6	8	3.32	0.624	5.320513
0.2	1.6	10	4.61	0.718667	6.414657

Freundlich

volume(L)	mass(g)	Ci(mg/L)	Ce(mg/L)	1/Ce	logCe	Qe	1/qe	log(qe)
0.2	1.5	2	0.35	2.857143	-0.45593	0.22	4.545455	-0.65758
0.2	1.5	4	0.75	1.333333	-0.12494	0.433333	2.307692	-0.36318
0.2	1.5	6	1.19	0.840336	0.075547	0.641333	1.559252	-0.19292
0.2	1.5	8	1.76	0.568182	0.245513	0.832	1.201923	-0.07988
0.2	1.5	10	2.49	0.401606	0.396199	1.001333	0.998668	0.000579

Appendix 3 First and second order Kinetics data

Time	Ci (mg/L)	Ce (mg/L)	qt (mg/g)	qe	t/qt	ln(qe-qt)
30	2	1.91235	0.011687	0.548	2567.028	-0.62304
60	2	1.365775	0.084563	0.548	709.5274	-0.76909
90	2	0.77	0.164581	0.548	546.8421	-0.95863

120	2	0.64674	0.180435	0.548	665.0607	-1.00085
150	2	0.86578	0.151229	0.548	991.8711	-0.9244

Appendix 4 Thermodynamics data

Temp	kelvin	1/T	kL	lnKL	R (J mol ⁻¹ K ⁻¹)	ΔG (j mol ⁻¹ k ⁻¹)	ΔG (KJ mol ⁻¹)
25	298	0.003356	2.42342	0.88518	8.314	-2193.096602	-2.193096602
30	303	0.0033	1.20564	0.187011	8.314	-471.1061216	-0.471106122
40	313	0.003195	0.65434	-0.42413	8.314	1103.701141	1.103701141

intercept	Slope	R ²	R (jmol ⁻¹ k ⁻¹)	ΔH (Kj mol ⁻¹)	ΔS (J k ⁻¹ mol ⁻¹)
7832.4	-25.503	0.954	8.314	0.21203194	65118.5736